Formation of Graphene p−n Superlattices on Pb Quantum Wedged Islands

Wenguang Zhu,[†,‡,*] Hua Chen,[†,‡] Kirk H. Bevan,[‡,§] and Zhenyu Zhang[⊥,†]

[†]Department of Physics and Astronomy, The University of Tennessee, Knoxville, Tennessee 37996, United States, [‡]Materials Science and Technology Division, Oak Ridge National Laboratory, Oak Ridge, Tennessee 37831, United States, [§]Centre for the Physics of Materials and Department of Physics, McGill University, Montreal PQ H3A 2T8, Canada, and [⊥]ICQD/HFNL, University of Science and Technology of China, Hefei, Anhui 230026, China.

ABSTRACT On the basis of first-principles calculations within density functional theory, we report on a novel scheme to create graphene p−n superlattices on Pb wedged islands with quantum stability. Pb(111) wedged islands grown on vicinal Si(111) extend over several Si steps, forming a wedged structure with atomically flat tops. The monolayer thickness variation due to the underlying substrate steps is a sizable fraction of the total thickness of the wedged islands and gives rise to a bilayer oscillation in the work function of Pb(111) due to quantum size effects. Here, we demonstrate that when a graphene sheet is placed on the surface of such a Pb wedged island, the spatial work function oscillation on the Pb wedged island surface caused by the underlying steps results in an oscillatory shift in the graphene Dirac point with respect to the Fermi level. Furthermore, by applying an external electric field of ∼0.5 V/Å in the surface normal direction, the Fermi level of the system can be globally tuned to an appropriate position such that the whole graphene layer becomes a graphene p−n superlattice of seamless junctions, with potentially exotic physical properties and intriguing applications in nanoelectronics.

KEYWORDS: graphene p−n superlattice · quantum size effects · graphene/metal contact

As conventional silicon-based semiconductor technology approaches its fabrication and operation limits, the demand for new materials and devices becomes increasingly pressing.[1] Graphene, owing to its simplicity and remarkable electronic transport properties, has recently emerged as a promising candidate material for future post-silicon electronics.[2] Its unusual linear energy dispersion gives rise to giant charge carrier mobility and a Dirac-like transport behavior, thereby enabling both fundamental studies of relativistic quantum phenomena and new device applications.[3−5] Notable exotic relativistic quantum phenomena, such as Klein tunneling,[6,7] Veselago lensing,[8] and guided plasmons,[9] have been theoretically predicted in graphene p−n junctions. More recently, it has also been predicted that a graphene p−n superlattice structure can lead to a number of fascinating new phenomena, including electron-beam supercollimation,[10] anisotropic transmission,[11] creation of additional Dirac cones,[12,13] and effective magnetic fields.[14] However, the creation of well-ordered and atomically sharp p−n junctions or superlattices remains practically challenging—though some prototype graphene p−n junctions have been experimentally demonstrated *via* local gating with costly and time-consuming e-beam lithographic techniques,[15−18] spatially selective chemical doping,[19] or electrostatic modification of the gate insulator surface.[20] Recent theoretical studies on the interaction between graphene and a series of metals indicate that metal-induced changes to the electrostatic potential in the graphene layer can result in net n- or p-type doping, depending on the work function of the metal surface.[21,22] Experimentally, epitaxial growth of high-quality graphene has been successfully demonstrated on a variety of metal substrates, which may serve as a rational synthesis route for producing macroscopic single-crystalline graphene.[23−30]

In this paper, we report on a novel scheme to create graphene p−n superlattices on Pb wedged islands by taking advantage of the spatial oscillations in the surface work function. The Pb wedged islands, schematically illustrated in Figure 1a, can be grown on Si(111) vicinal substrates at room temperature.[31] These islands have an atomically flat top oriented in the [111] direction driven by surface energy minimization,[32,33] but their bottom extends laterally over several atomic steps on the Si vicinal substrate. Thus each Pb wedged island contains striped regions consecutively increasing in thickness, and more importantly, the width of the stripes is solely determined by the experimentally tunable terrace width of the underlying Si vicinal substrate. Such wedged islands provide an

* Address correspondence to wzhu3@utk.edu.

Received for review January 5, 2011 and accepted April 7, 2011.

Published online April 07, 2011
10.1021/nn200052f

ideal platform for studying the influence of quantum size effects on the physical and chemical properties of the materials adsorbed on top of the quantum wedge.[34−37] Previous first-principles calculations and scanning tunneling spectroscopy (STS) measurements have shown that Pb(111) films exhibit a bilayer work function oscillation (see Figure 1b), which arises from the unique matching between the bulk Pb Fermi wavelength and the Pb(111) interlayer lattice spacing.[38−41] Here, we use first-principles calculations within density functional theory to demonstrate that, when a single layer of graphene is placed on the surface of such a Pb wedged island, the spatial oscillations in the surface work function will induce a corresponding oscillation in the position of the graphene Dirac point relative to the Fermi level of the system. Furthermore, by applying an external electric field of 0.5 V/Å perpendicular to the surface the graphene Fermi level can be globally tuned to an appropriate position, such that the whole graphene layer becomes a well-defined graphene p−n superlattice with seamless junctions.

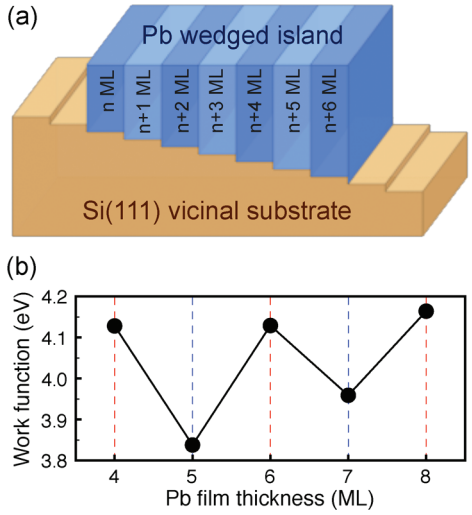

Figure 1. (a) Schematic illustration of a Pb wedged island grown on a Si(111) vicinal substrate. (b) Work function of Pb(111) films calculated within density functional theory as a function of the film thickness.

RESULTS AND DISCUSSION

We begin this study by searching for the stable adsorption geometries of graphene on Pb(111) films. To this end, a number of possible configurations have been considered in our study. Images a and b of Figure 2 show the two most stable structures, which are nearly degenerate in energy. Their relative stability depends on the Pb film thickness, but their total energy difference is less than 0.02 eV for all cases studied. Even with the most stable structures, graphene is weakly adsorbed (physisorbed) on the Pb(111) films; the calculated binding energies are around 0.026 eV per carbon atom, and the average equilibrium separation

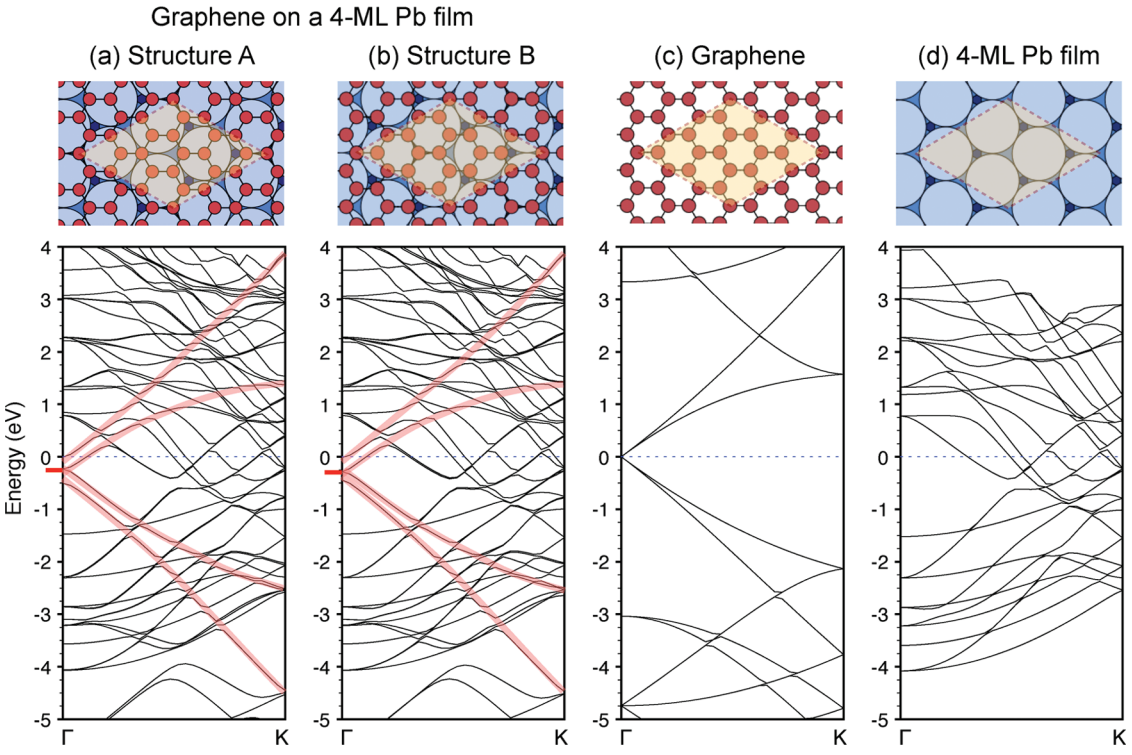

Figure 2. Atomic structures and calculated band structures of the two most stable configurations of graphene on 4-ML Pb(111) films (a,b), a single layer of graphene (c), and a 4-ML Pb(111) film (d). Red and blue balls represent C and Pb atoms, respectively. The Fermi levels are set to zero in the band structure plots, as denoted by blue dashed lines. In the graphene/Pb combined systems (a,b), the graphene band structure is highlighted *via* transparent red curves, and red short bars attached to the energy axis indicate the positions of the graphene Dirac point.

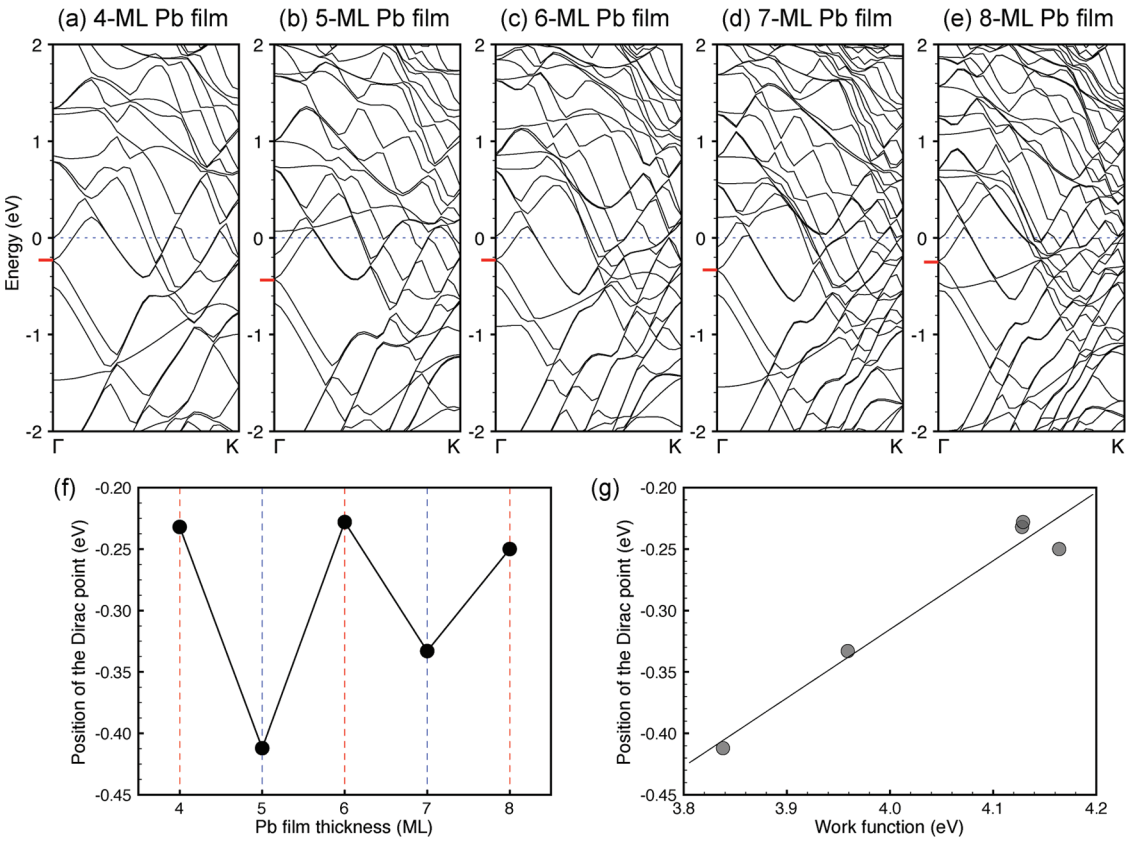

Figure 3. Band structure of graphene on 4- to 8-ML Pb(111) films (a−e). The Fermi levels are set to zero in the band structure plots, as denoted by blue dashed lines. (f) Positions of the graphene Dirac point with respect to the Fermi level as a function of the thickness of the underlying 4- to 8-ML Pb films. (g) Correlation between the position of the Dirac point and the work function of the Pb films.

between graphene and the Pb(111) surface is around 3.6 Å for all film thicknesses.[21,22]

To identify changes in the electronic structure of graphene occurring upon Pb(111) adsorption, we have calculated the band structure of graphene atop a 4-ML Pb(111) film at both of the stable adsorption geometries (as illustrated in Figure 2a,b). The energy bands arising from graphene can be identified in the combined system by comparing the band structure of free-standing graphene (see Figure 2c) with that of an isolated 4-ML Pb(111) film (see Figure 2d). Since a 3×3 graphene unit cell is used in the calculations, the 1×1 unit cell K points in reciprocal space are folded onto the Γ point. The absorbed graphene band splitting at the Γ point results from the periodic substrate-induced corrugation, which introduces electronic coupling between the two distinct Dirac cone valleys of flat graphene. Nevertheless, the Dirac cone of graphene is largely preserved because flat strained graphene adsorbed on Pb(111) films and the two relaxed minimum structures give nearly identical shifts in the graphene Dirac point with respect to the Fermi level of the system. Similar calculations have also been carried out for 5−8 ML Pb(111) films. Figure 3a−e shows the band structure of graphene atop 4−8 ML Pb films, respectively. Since the two stable adsorption geometries have nearly identical band structures, only the plots for the structure A (see Figure 2a) are presented in Figure 3 for comparison. In Figure 3f, the position of the graphene Dirac point is plotted as a function of the Pb(111) substrate film thickness, and a clear bilayer oscillation in the Dirac point is evident (due to the work function oscillation in the underlying Pb films). A linear relationship between the position of the graphene Dirac point and the work function of the Pb films is revealed in Figure 3g. However, the graphene Dirac point lies below the Fermi level at all film thicknesses, and electrons are donated from the Pb films to graphene, making graphene n-type doped. This can be attributed to the relatively small work function of Pb(111) (∼4 eV). Previous calculations indicate that the crossover from n-type to p-type doping occurs for a metal work function of ∼5.4 eV.[21,22]

To achieve a graphene p−n superlattice, the Fermi level of graphene needs to be shifted downward. One possible way to achieve this is through an external electric field applied perpendicular to the surface, as schematically illustrated in Figure 4a, such that some screening electrons on graphene are forced back into the Pb substrate and consequently shift the graphene Fermi level downward. To quantitatively determine the critical magnitude of the electric field required to form

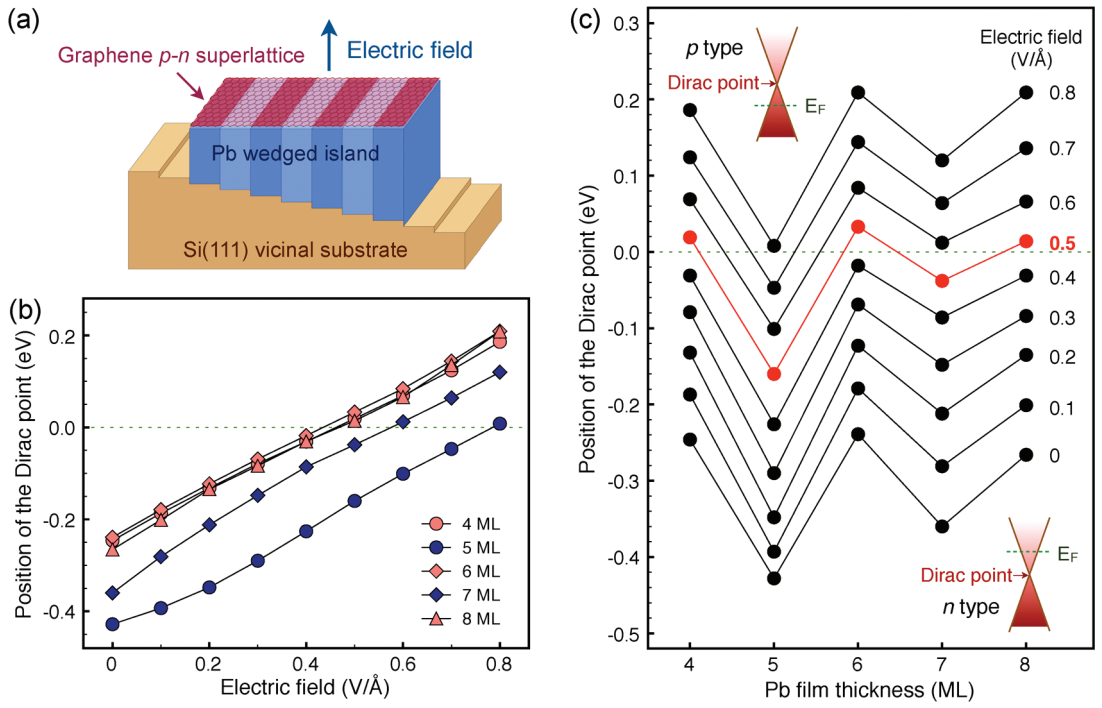

Figure 4. (a) Schematic illustration of a graphene p−n superlattice formed on a Pb wedged island with an external electric field applied in the surface normal direction. (b,c) Evolution of the graphene Dirac point position plotted as a function of the electric field (b) and the Pb film thickness (c). The Fermi level is set to zero in all plots and denoted by green dashed lines.

a graphene p−n superlattice on a Pb wedged island, we have included an electric field in the surface normal direction ranging from 0.1 to 0.8 V/Å in our first-principles calculations. The results for film thicknesses from 4 to 8 MLs, presented in Figure 4b, indicate that the Dirac point position is elevated approximately linearly with respect to the external electric field magnitude. To better illustrate the evolution of the Dirac point shifts and to identify the critical magnitude of the electric field required to achieve a graphene p−n superlattice, the same set of data is plotted as a function of the Pb film thickness at different electric fields (see Figure 4c). From this plot, it is evident that the graphene Dirac points (for all film thickness) are simultaneously pushed upward by the applied field and that a critical electric field of around 0.5 V/Å is required to form a graphene p−n superlattice on a Pb wedged island, which is comparable to the field strength applied to open a band gap in bilayer graphene as recently demonstrated experimentally.[42]

It should be noted that instead of modeling a Pb wedged island we used flat Pb films of different thicknesses and performed the calculations separately. On a real Pb wedged island, it is expected that some charges will accumulate at the interfaces between the Pb stripe regions with different work functions. Such interface charge accumulation will create a local electric field at the interface and thereby balance the Fermi level difference between two adjacent regions. However, at a particular small region, the shift of the graphene Dirac point relative to the local Fermi level is solely determined by the local work function of the Pb surface and the uniform external electric field. Therefore, given the short screening length of Pb as a metal (~0.75 nm as shown in Figure 5a), as evident from the experimental STS work function measurements,[40,41] the interface charge accumulation is not expected to invalidate our proposed scheme of creating graphene p−n superlattices on Pb wedged islands, as long as the width of each Pb stripe region is approximately three times greater than the screening length of Pb to ensure well-defined p−n regions.[40,41]

The correlation between the graphene Fermi level position and the external electric field magnitude can be understood using a phenomenological parallel plate capacitor model, such as that given in refs 21 and 22. There, the work function difference between graphene and the substrate is balanced by (1) the classical capacitance of the capacitor (*i.e.*, the potential difference developed due to charge redistribution between two plates) plus the charging energy of each plate, and (2) the quantum capacitance of graphene (*i.e.*, the Fermi level shift relative to the Dirac point). In refs 21 and 22, the authors take the charge redistribution in (1) equal to the amount calculated by integrating the graphene density of states in the range swept by the Fermi level. However, in the following, we point out that this parallel plate picture is not entirely accurate when graphene and the substrate are in direct contact, such that the overlap between the "spilled-out" charge is non-negligible.

To clearly visualize the charge redistribution upon application of an external electric field, we plot the

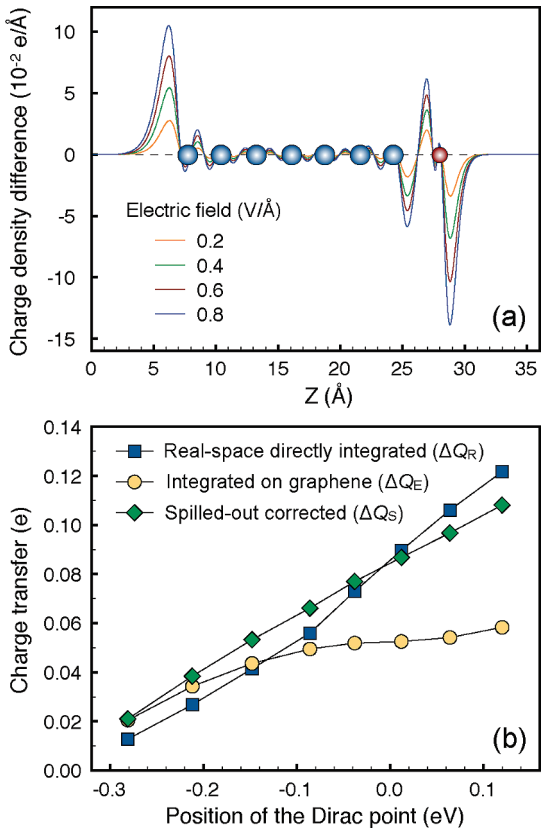

Figure 5. (a) Electron screening charge for a graphene layer placed on a 7-ML Pb(111) film. The screening charge density is integrated in the plane parallel to the Pb(111) film and plotted in the perpendicular direction. Red and blue balls indicate the positions of C and Pb layers, respectively. (b) Amount of charge transferred out of the graphene *versus* the position of the Dirac point. Blue squares (ΔQ_R) are the total screening charge density integrated in real space from the zero point halfway between graphene and the Pb film into the vacuum. Yellow dots (ΔQ_E) are the amount of charge transfer estimated from integrating the graphene DOS in the range swept by the Fermi level. Green diamonds (ΔQ_S) are the summed screen charges of isolated graphene and the isolated Pb film (integrated in the same manner as ΔQ_R).

plane-integrated electron density screening charge of graphene on a 7-ML Pb film in Figure 5a at various electric field intensities. As expected, the applied electric field pushes electrons from graphene to Pb, and this screening charge transfer increases with the applied electric field magnitude. We then integrate screening charge in Figure 5a from the zero point halfway between graphene and Pb to the vacuum above graphene where the screening charge density vanishes. This amount of charge ΔQ_R (R for real space) is physically "on" the plate of graphene and is analogous to the charge redistribution between two parallel plates in a classical capacitor. For comparison, we also calculated ΔQ_E (E for energy space) by integrating the graphene density of states in the range swept by the Fermi level (upon applying an external field). The results are depicted in Figure 5b, and one can see that ΔQ_E significantly underestimates the charge redistribution in the real space. This is because ΔQ_E does not take into account the tail of the spilled-out charge from Pb, which extends over the gap region between graphene and Pb and contributes to screening the external field inside the gap. To better support our statement, we separately calculated the screening charge redistribution of both graphene and the 7-ML Pb film in isolation (with their respective geometries fixed). We then properly combine the two isolated screening charge densities and perform integration in the same spatial range as we did for ΔQ_R. Within the graphene–Pb gap, this charge counting scheme is analogous to a phenomenological WKB model. The resulting ΔQ_S quantity (S for spilled-out charge correction) is also shown in Figure 5b and agrees well with ΔQ_R.

As a final remark, we would like to point out that the proposed graphene p–n superlattice mechanism relies on the spatial oscillation of the surface work function of *metallic* Pb wedged islands. Hence with respect to graphene transport measurements, such *metallic* islands can form an electrical short and are therefore only appropriate for ballistic conduction measurements when the islands are not connected to the electron source or drain injecting electrons/holes into graphene. The absence of Pb electronic states at the graphene Dirac point and the weakness of the graphene–Pb physisobtion interaction provide minimal electronic coupling between conducting graphene electrons and Pb (see Figures 2 and 3).[43] Therefore, the probability of electrons injected directly into graphene (and not into Pb) subsequently scattering into an isolated Pb(111) donor/acceptor substrate can be made negligible at sufficiently low temperatures (where inelastic scattering into Pb is minimized) and at distances less than a mean free path.[44] Additionally, we propose that this superlattice structure might possibly be preserved through delicate chemical modifications. Previous experimental studies have demonstrated that the surfaces of Pb(111) wedged islands exhibit spatial oscillatory chemical reactivity[35] and adsorbate binding,[37] due to the same quantum size effects highlighted in this work. Similar tunable chemical behavior may also exist on the surface of a graphene p–n superlattice when it is placed atop a Pb wedged island. Once such a graphene layer is chemically modified, *via* selective reactions or adsorbate bindings within the oscillatorily doped regions, the superlattice structure might then be preserved even after it is lifted from the Pb wedged island for further chemical modifications to create other types of graphene-based superlattices, as a new way of achieving graphene band engineering. This strategy is similar to a recent proposal to create hydrogenated graphene superlattices *via* selective H adsorption on strain-engineered nanoripples.[45] The validity of this speculation requires further extensive studies to confirm.

CONCLUSIONS

In summary, we have demonstrated a novel scheme to create atomically sharp graphene p−n superlattices on Pb quantum wedged islands induced by an external electric field. To achieve such a graphene p−n superlattice, a critical external electric field of ~0.5 V/Å has been estimated based on first-principles density functional theory calculations. The relationship between the graphene Fermi level position and the external electric field magnitude has been quantitatively analyzed using a phenomenological parallel plate capacitor model. This finding may provide an effective approach to virtually divide a single graphene layer into stripe regions with distinctive electronic and chemical properties of well-controlled width, offering a novel route to potentially create graphene-based superlattices with innovative applications such as electron-beam supercollimation.[10]

METHODS

Our first-principles density functional theory calculations were carried out using the VASP code,[46] with the projector augmented wave (PAW) method applied to describe the electron−ion interactions.[47,48] The local density approximation (LDA)[49] was used to approximate electron exchange and correlation, as it provides a much better description of the graphene−metal binding energy and equilibrium separation than the generalized gradient approximation (GGA).[22] The plane-wave kinetic energy cutoff was set at 400 eV. The lattice constants of bulk Pb and graphene determined with these computational approximations are 4.879 and 2.446 Å, respectively, which are in good agreement with the experimental values of 4.95 and 2.46 Å. The Pb films were modeled by periodic slabs consisting of 4−8 monolayers (MLs), separated by a vacuum region of 18 Å. To match graphene on the Pb films, we constructed a 2×2 Pb(111) surface cell and placed a 3×3 graphene layer on top, resulting in a mismatch of around 6%. We set the in-plane lattice constant of Pb(111) at its optimized LDA value and adapted the lattice of graphene accordingly. In optimizing the geometry, the bottom monolayer Pb atoms were fixed at their bulk positions, and all other atoms were allowed to relax until the forces on all the unconstrained atoms were smaller in magnitude than 0.01 eV/Å. To include the effect of an external electric field, an artificial dipole layer was placed in the middle of the vacuum region far away from either side of the slab.[50,51]

Acknowledgment. This work was supported by the Division of Materials Science and Engineering, Office of Basic Energy Sciences, U.S. Department of Energy, and in part by NSF Grant No. 0906025 and NSERC of Canada. The calculations were performed at NERSC of DOE.

REFERENCES AND NOTES

1. Osborne, I.; Lavine, M.; Coontz, R. Looking beyond Silicon. *Science* **2010**, *327*, 1595.
2. Schwierz, F. Graphene Transistors. *Nat. Nanotechnol.* **2010**, *5*, 487–496.
3. Geim, A. K.; Novoselov., K. S. The Rise of Graphene. *Nat. Mater.* **2007**, *6*, 183–191.
4. Geim, A. K. Graphene: Status and Prospects. *Science* **2009**, *324*, 1530–1534.
5. Castro Neto, A. H.; Guinea, F.; Peres, N. M. R.; Novoselov, K. S.; Geim, A. K. The Electronic Properties of Graphene. *Rev. Mod. Phys.* **2009**, *81*, 109–162.
6. Katsnelson, M. I.; Novoselov, K. S.; Geim, A. K. Chiral Tunnelling and the Klein Paradox in Graphene. *Nat. Phys.* **2006**, *2*, 620–625.
7. Beenakker, C. W. J. Colloquium: Andreev Reflection and Klein Tunneling in Graphene. *Rev. Mod. Phys.* **2008**, *80*, 1337–1354.
8. Cheianov, V. V.; Fal'ko, V.; Altshuler, B. L. The Focusing of Electron Flow and a Veselago Lens in Graphene p−n Junctions. *Science* **2007**, *315*, 1252–1255.
9. Mishchenko, E. G.; Shytov, A. V.; Silvestrov, P. G. Guided Plasmons in Graphene p−n Junctions. *Phys. Rev. Lett.* **2010**, *104*, 156806.
10. Park, C.-H.; Son, Y.-W.; Yang, L.; Cohen, M. L.; Louie, S. G. Electron Beam Supercollimation in Graphene Superlattices. *Nano Lett.* **2008**, *8*, 2920–2924.
11. Park, C.-H.; Yang, L.; Son, Y.-W.; Cohen, M. L.; Louie, S. G. Anisotropic Behaviours of Massless Dirac Fermions in Graphene under Periodic Potentials. *Nat. Phys.* **2008**, *4*, 213–217.
12. Park, C.-H.; Son, Y.-W.; Yang, L.; Cohen, M. L.; Louie, S. G. Landau Levels and Quantum Hall Effect in Graphene Superlattices. *Phys. Rev. Lett.* **2009**, *103*, 046808.
13. Brey, L.; Fertig, H. A. Emerging Zero Modes for Graphene in a Periodic Potential. *Phys. Rev. Lett.* **2009**, *103*, 046809.
14. Sun, J. M.; Fertig, H. A.; Brey, L. Effective Magnetic Fields in Graphene Superlattices. *Phys. Rev. Lett.* **2010**, *105*, 156801.
15. Williams, J. R; DiCarlo, L.; Marcus, C. M. Quantum Hall Effect in a Gate-Controlled p−n Junction of Graphene. *Science* **2007**, *317*, 638–641.
16. Huard, B.; Sulpizio, J. A.; Stander, N.; Todd, K.; Yang, B.; Goldhaber-Gordon, D. Transport Measurements Across a Tunable Potential Barrier in Graphene. *Phys. Rev. Lett.* **2007**, *98*, 236803.
17. Özyilmaz, B.; Jarillo-Herrero, P.; Efetov, D.; Kim, P. Electronic Transport in Locally Gated Graphene Nanoconstrictions. *Appl. Phys. Lett.* **2007**, *91*, 192107.
18. Liu, G.; Velasco, J., Jr.; Bao, W. Z.; Lau, C. N. Fabrication of Graphene p−n−p Junctions with Contactless Top Gates. *Appl. Phys. Lett.* **2008**, *92*, 203103.
19. Lohmann, T.; von Klitzing, K.; Smet, J. H. Four-Terminal Magneto-Transport in Graphene p−n Junctions Created by Spatially Selective Doping. *Nano Lett.* **2009**, *9*, 1973–1979.
20. Chiu, H.-Y.; Perebeinos, V.; Lin, Y.-M.; Avouris, Ph. Controllable p−n Junction Formation in Monolayer Graphene Using Electrostatic Substrate Engineering. *Nano Lett.* **2010**, *10*, 4634–4639.
21. Giovannetti, G.; Khomyakov, P. A.; Brocks, G.; Karpan, V. M.; van den Brink, J.; Kelly, P. J. Doping Graphene with Metal Contacts. *Phys. Rev. Lett.* **2008**, *101*, 026803.
22. Khomyakov, P. A.; Giovannetti, G.; Rusu, P. C.; Brocks, G.; van den Brink, J.; Kelly, P. J. First-Principles Study of the Interaction and Charge Transfer between Graphene and Metals. *Phys. Rev. B* **2009**, *79*, 195425.
23. Wintterlin, J.; Bocquet, M.-L. Graphene on Metal Surfaces. *Surf. Sci.* **2009**, *603*, 1841–1852.
24. Sutter, P. W.; Flege, J.-I.; Sutter, E. A. Epitaxial Graphene on Ruthenium. *Nat. Mater.* **2008**, *7*, 406–411.
25. Pan, Y.; Zhang, H. G.; Shi, D. X.; Sun, J. T.; Du, S. X.; Liu, F.; Gao, H.-J. Highly Ordered, Millimeter-Scale, Continuous, Single-Crystalline Graphene Monolayer Formed on Ru (0001). *Adv. Mater.* **2009**, *21*, 2777–2780.
26. Kim, K. S.; Zhao, Y.; Jang, H.; Lee, S. Y.; Kim, J. M.; Kim, K. S.; Ahn, J.-H.; Kim, P.; Choi, J.-Y.; Hong, B. H. Large-Scale Pattern Growth of Graphene Films for Stretchable Transparent Electrodes. *Nature* **2009**, *457*, 706–710.
27. Li, X. S.; Cai, W. W.; An, J. H.; Kim, S.; Nah, J.; Yang, D. X.; Piner, R.; Velamakanni, A.; Jung, I.; Tutuc, E.; *et al.* Large-Area Synthesis of High-Quality and Uniform Graphene Films on Copper Foils. *Science* **2009**, *324*, 1312–1314.

28. Coraux, J.; N'Diaye, A. T.; Busse, C.; Michely, T. Structural Coherency of Graphene on Ir(111). *Nano Lett.* **2008**, *8*, 565–570.
29. Li, X. S.; Cai, W. W.; Colombo, L.; Ruoff, R. S. Evolution of Graphene Growth on Ni and Cu by Carbon Isotope Labeling. *Nano Lett.* **2009**, *9*, 4268–4272.
30. Loginova, E.; Bartelt, N. C.; Feibelman, P. J.; McCarty, K. F. Factors Influencing Graphene Growth on Metal Surfaces. *New J. Phys.* **2009**, *11*, 063046.
31. Altfeder, I. B.; Matveev, K. A.; Chen, D. M. Electron Fringes on a Quantum Wedge. *Phys. Rev. Lett.* **1997**, *78*, 2815–2818.
32. Okamoto, H.; Chen, D. M.; Yamada, T. Competing Classical and Quantum Effects in Shape Relaxation of a Metallic Island. *Phys. Rev. Lett.* **2002**, *89*, 256101.
33. Li, S.-C.; Ma, X. C.; Jia, J.-F.; Zhang, Y.-F.; Chen, D. M.; Niu, Q.; Liu, F.; Weiss, P. S.; Xue, Q.-K. Influence of Quantum Size Effects on Pb Island Growth and Diffusion Barrier Oscillations. *Phys. Rev. B* **2006**, *74*, 075410.
34. Guo, Y.; Zhang, Y.-F.; Bao, X.-Y.; Han, T.-Z.; Tang, Z.; Zhang, L.-X.; Zhu, W. G.; Wang, E. G.; Niu, Q.; Qiu, Z. Q.; *et al.* Superconductivity Modulated by Quantum Size Effects. *Science* **2004**, *306*, 1915–1917.
35. Ma, X. C.; Jiang, P.; Qi, Y.; Jia, J.-F.; Yang, Y.; Duan, W. H.; Li, W.-X.; Bao, X. H.; Zhang, S. B.; Xue, Q.-K. Experimental Observation of Quantum Oscillation of Surface Chemical Reactivities. *Proc. Natl. Acad. Sci. U.S.A.* **2007**, *104*, 9204–9208.
36. Ma, L.-Y.; Tang, L.; Guan, Z.-L.; He, K.; An, K.; Ma, X.-C.; Jia, J.-F.; Xue, Q.-K.; Han, Y.; Huang, S.; *et al.* Quantum Size Effect on Adatom Surface Diffusion. *Phys. Rev. Lett.* **2006**, *97*, 266102.
37. Jiang, P.; Ma, X. C.; Ning, Y. X.; Song, C. L.; Chen, X.; Jia, J.-F.; Xue., Q.-K. Quantum Size Effect Directed Selective Self-Assembling of Cobalt Phthalocyanine on Pb(111) Thin Films. *J. Am. Chem. Soc.* **2008**, *130*, 7790–7791.
38. Wei, C. M.; Chou, M. Y. Theory of Quantum Size Effects in Thin Pb(111) Films. *Phys. Rev. B* **2002**, *66*, 233408.
39. Jia, Y.; Wu, B.; Weitering, H. H.; Zhang, Z. Y. Quantum Size Effects in Pb Films from First Principles: The Role of the Substrate. *Phys. Rev. B* **2006**, *74*, 035433.
40. Qi, Y.; Ma, X. C.; Jiang, P.; Ji, S. H.; Fu, Y. S.; Jia, J.-F.; Xue, Q.-K.; Zhang, S. B. Atomic-Layer-Resolved Local Work Functions of Pb Thin Films and Their Dependence on Quantum Well States. *Appl. Phys. Lett.* **2007**, *90*, 013109.
41. Kim, J.; Qin, S. Y.; Yao, W.; Niu, Q.; Chou, M. Y.; Shih, C.-K. Quantum Size Effects on the Work Function of Metallic Thin Film Nanostructures. *Proc. Natl. Acad. Sci. U.S.A.* **2010**, *107*, 12761–12765.
42. Zhang, Y. B.; Tang, T.-T.; Girit, C.; Hao, Z.; Martin, M. C.; Zettl, A.; Crommie, M. F.; Shen, Y. R.; Wang, F. Direct Observation of a Widely Tunable Bandgap in Bilayer Graphene. *Nature* **2009**, *459*, 820–823.
43. Karpan, V. M.; Giovannetti, G.; Khomyakov, P. A.; Talanana, M.; Starikov, A. A.; Zwierzycki, M.; van den Brink, J.; Brocks, G.; Kelly, P. J. Graphite and Graphene as Perfect Spin Filters. *Phys. Rev. Lett.* **2007**, *99*, 176602.
44. Novoselov, K. S.; Geim, A. K.; Morozov, S. V.; Jiang, D.; Katsnelson, M. I.; Grigorieva, I. V.; Dubonos, S. V.; Firsov, A. A. Two-Dimensional Gas of Massless Dirac Fermions in Graphene. *Nature* **2005**, *438*, 197–200.
45. Wang, Z. F.; Zhang, Y.; Liu, F. Formation of Hydrogenated Graphene Nanoripples by Strain Engineering and Directed Surface Self-Assembly. *Phys. Rev. B* **2011**, *83*, 041403(R).
46. Kresse, G.; Furthmüller, J. Efficient Iterative Schemes for *Ab Initio* Total-Energy Calculations Using a Plane-Wave Basis Set. *Phys. Rev. B* **1996**, *54*, 11169–11186.
47. Blöchl, P. E. Projector Augmented-Wave Method. *Phys. Rev. B* **1994**, *50*, 17953–17979.
48. Kresse, G.; Joubert, D. From Ultrasoft Pseudopotentials to the Projector Augmented-Wave Method. *Phys. Rev. B* **1999**, *59*, 1758–1775.
49. Perdew, J. P.; Zunger, A. Self-Interaction Correction to Density-Functional Approximations for Many-Electron Systems. *Phys. Rev. B* **1981**, *23*, 5048–5079.
50. Neugebauer, J.; Scheffler, M. Adsorbate–Substrate and Adsorbate–Adsorbate Interactions of Na and K Adlayers on Al(111). *Phys. Rev. B* **1992**, *46*, 16067–16080.
51. Makov, G.; Payne, M. C. Periodic Boundary Conditions in *Ab Initio* Calculations. *Phys. Rev. B* **1995**, *51*, 4014–4022.